Electronic Supplementary Information

Membrane-controlled CO_2 Electrocatalysts with Switchable C2 Product Selectivity and High Faradaic Efficiency for Ethanol

Tania Akter[a] and Christopher J. Barile[a*]

[a] Department of Chemistry, University of Nevada, Reno

*E-mail: cbarile@unr.edu

Supplementary Figures

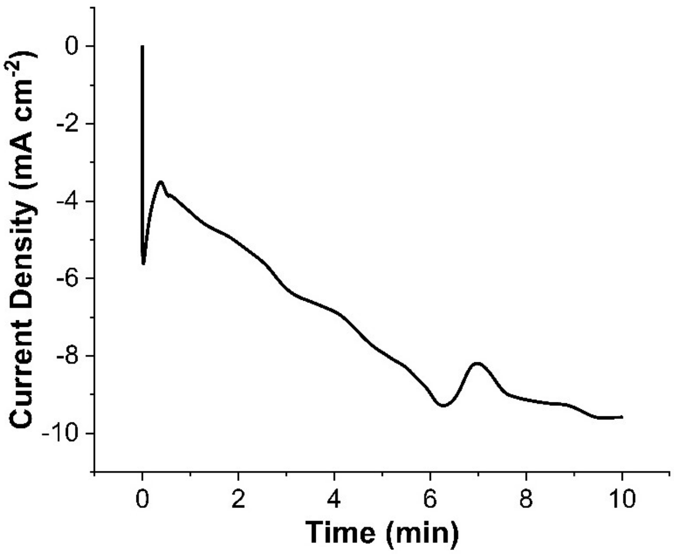

Figure S1: Representative chronoamperometry curve of Cu deposition on Ag surface at -3 V vs. Ag/AgCl in 50 mM $CuSO_4$.

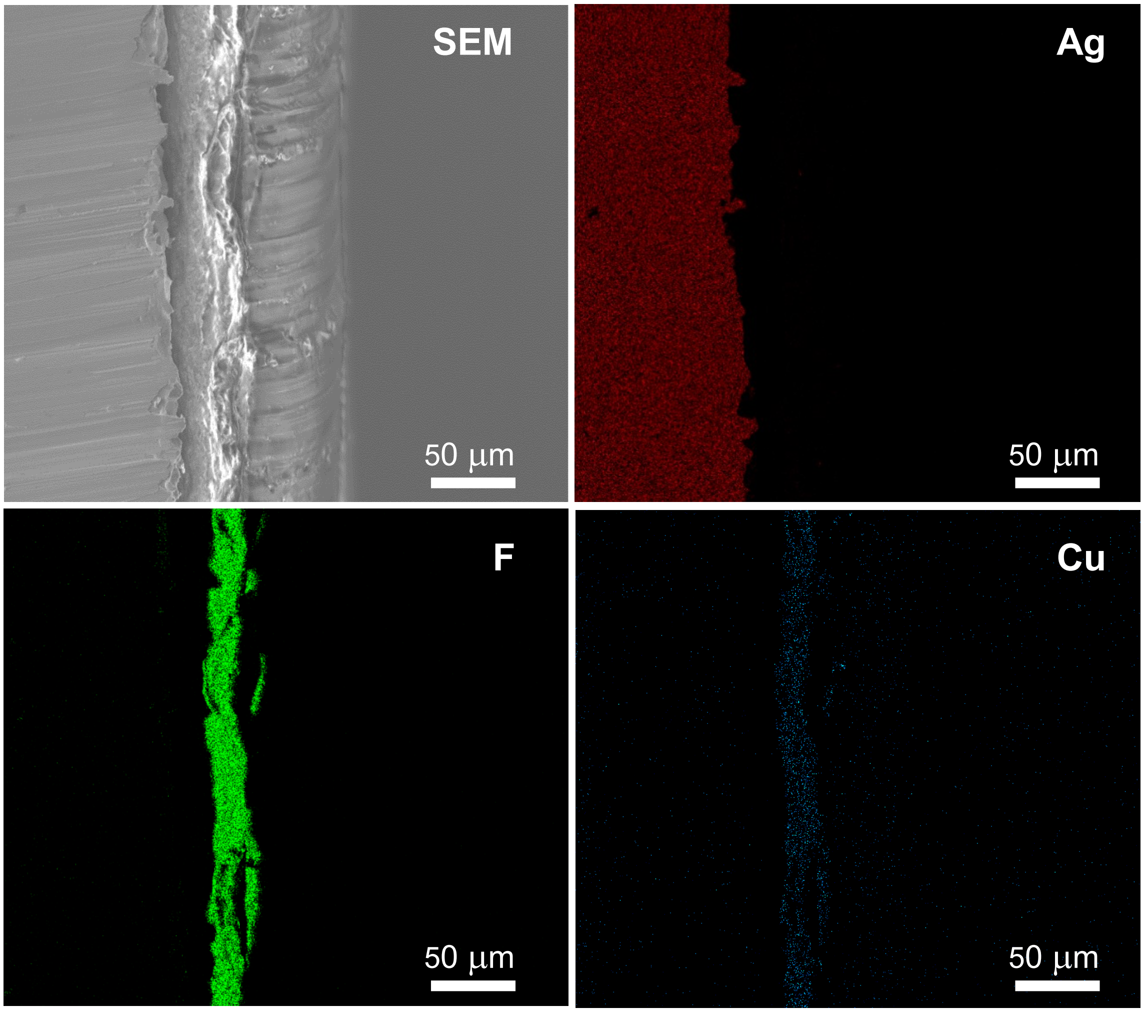

Figure S2: SEM image and corresponding EDX elemental maps for Ag, F, and Cu of a Nafion fabricated Ag-Cu electrode.

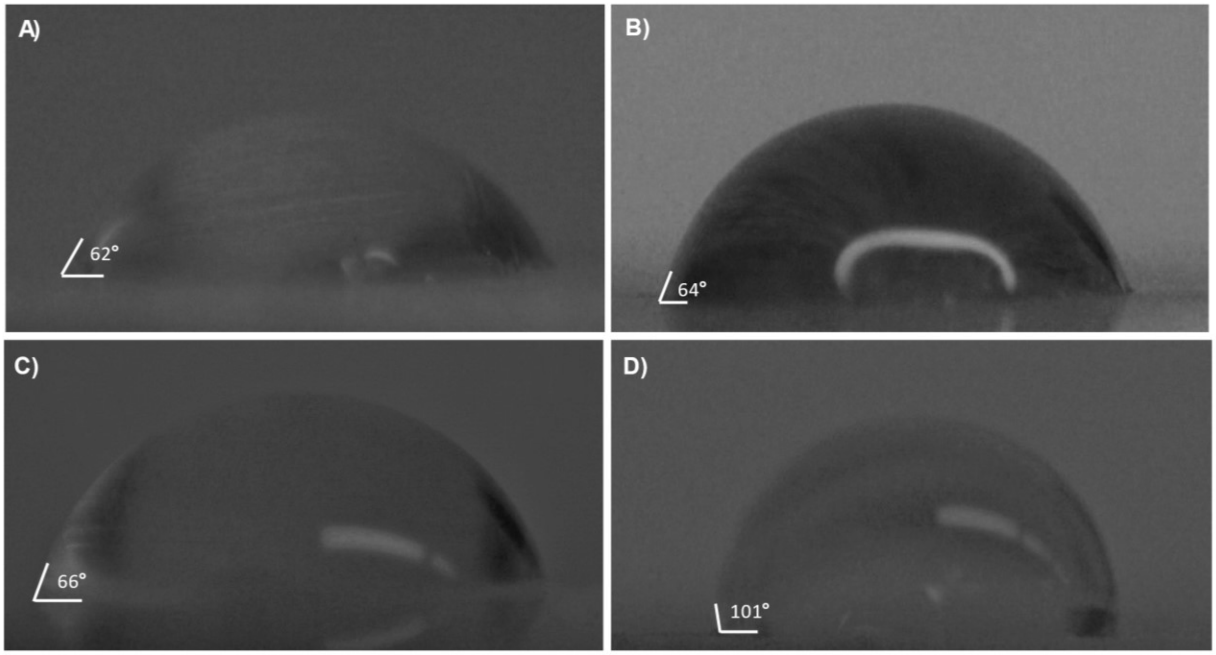

Electrodes	Angle (degrees)
Ag-Cu	62 ± 1
Ag-Cu/Aquivion	64 ± 2
Ag-Cu/Nafion	66 ± 3
Ag-Cu/Nafion-PVDF	101 ± 2

Figure S3: Representative photographs of water droplets on unmodified Ag-Cu (A) and Ag-Cu electrodes modified with Aquivion (B), Nafion (C), and 5.0 wt % PVDF with Nafion (D). The corresponding contact angles are displayed in the table.

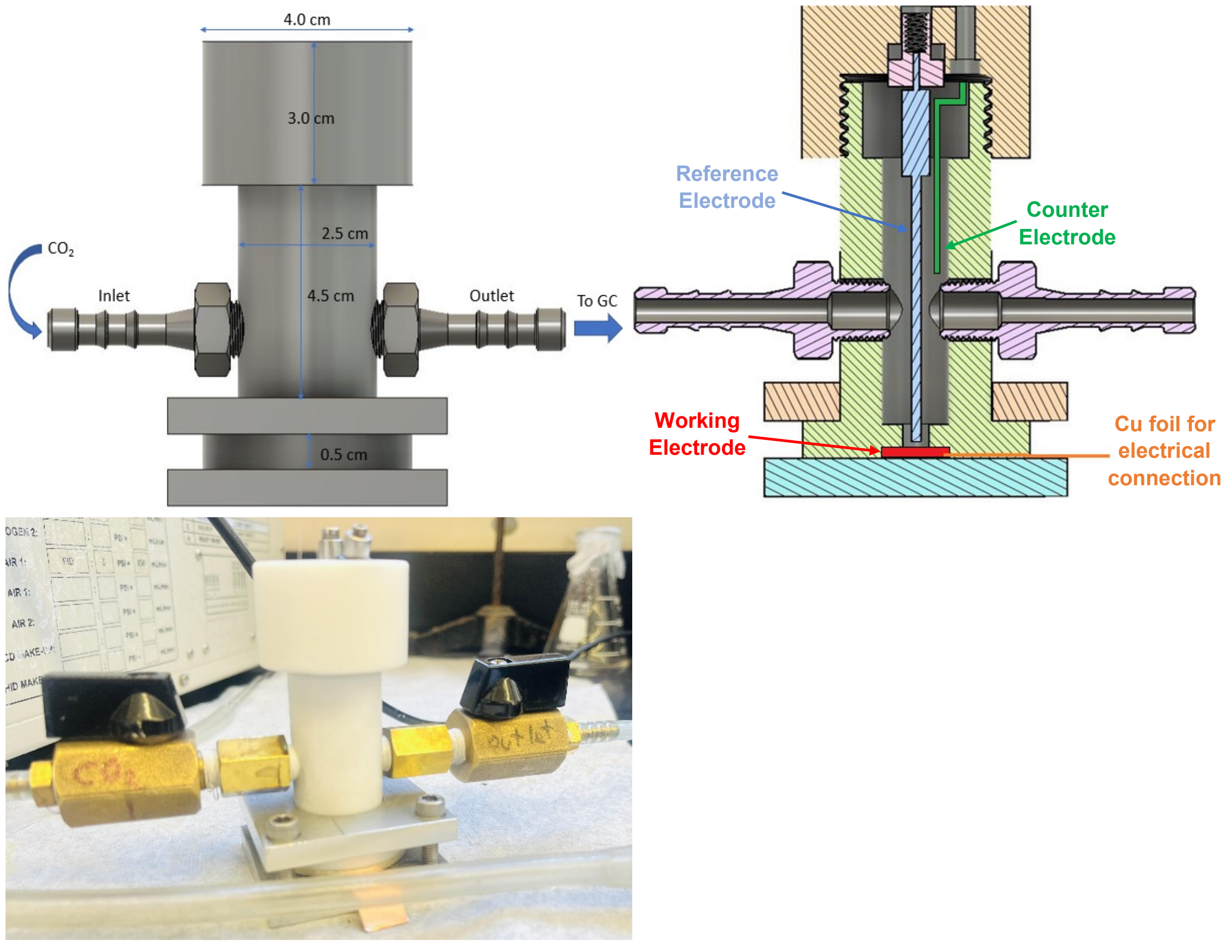

Figure S4: Diagram and photograph of cell used for gas collection and subsequent detection using gas chromatography. The working electrode size was 5.0 cm^2. The counter electrode was 3.0 cm in length and consisted of Pt wire 1.0 mm in diameter. The counter and reference electrodes were inserted into the cell via ports in the Teflon cell cap and were hermetically sealed with o-rings. The reference and counter were 0.5 cm apart from each other and from the working electrode. The working electrode was positioned on the cell bottom and was also sealed with an o-ring. Gaseous products were transferred from the cell by using a 20 mL glass gas syringe to the GC for analysis.

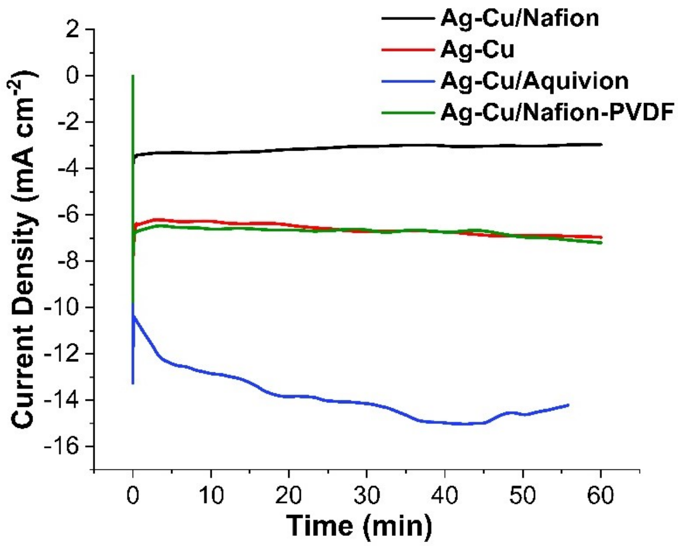

Figure S5: Representative chronoamperometry curves of CO_2 reduction at -1.9 V vs. RHE using Ag-Cu electrode modified with Nafion (black), Aquivion (blue), and Nafion-PVDF (green) along with unmodified Ag-Cu (red).

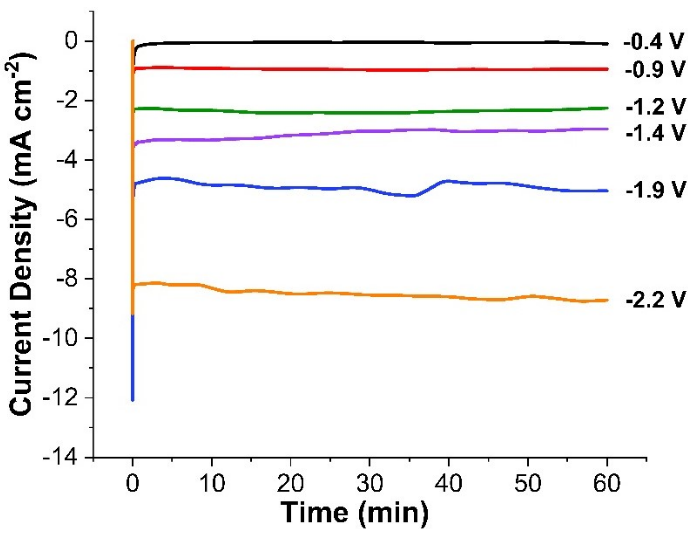

Figure S6: Representative chronoamperometry curves of CO_2 reduction at several voltages vs. RHE using a Ag-Cu electrode modified with 16 μm of Nafion.

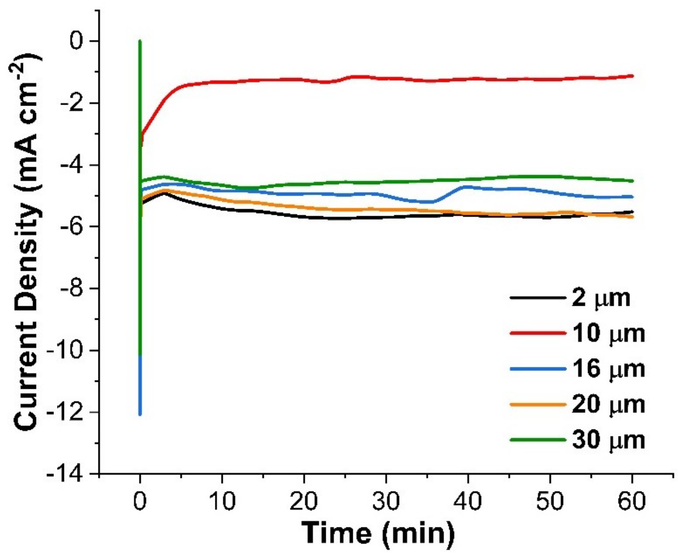

Figure S7: Representative chronoamperometry curves of CO_2 reduction at -1.2 V vs. RHE using Ag-Cu electrodes modified with various thicknesses of Nafion.

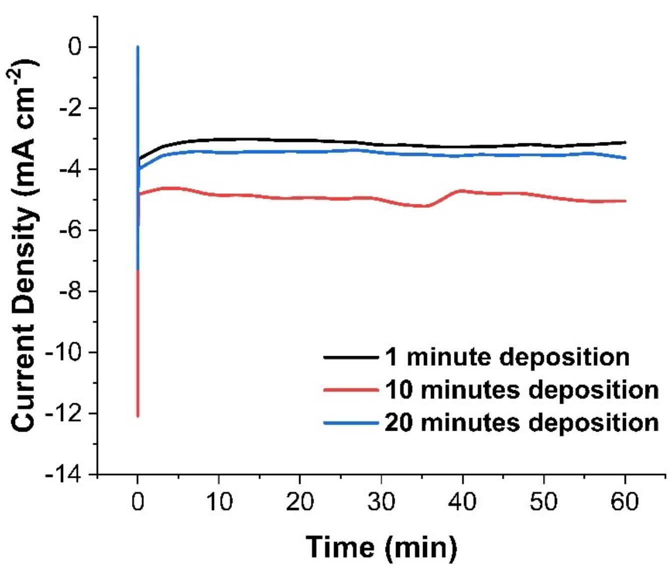

Figure S8: Representative chronoamperometry curves of CO_2 reduction at -1.2 V vs. RHE of Ag-Cu electrodes modified with 16 μm of Nafion in which Cu was deposited for 1 min (black), 10 min (red), and 20 min (blue).

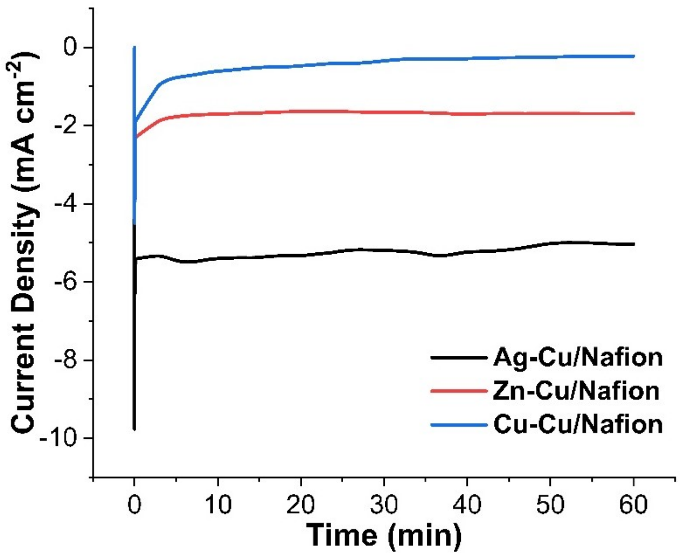

Figure S9: Representative chronoamperometry curves of CO_2 reduction at -1.2 V vs. RHE of Ag-Cu (black), Cu-Cu (blue), and Zn-Cu (red) electrodes modified with 16 μm of Nafion.

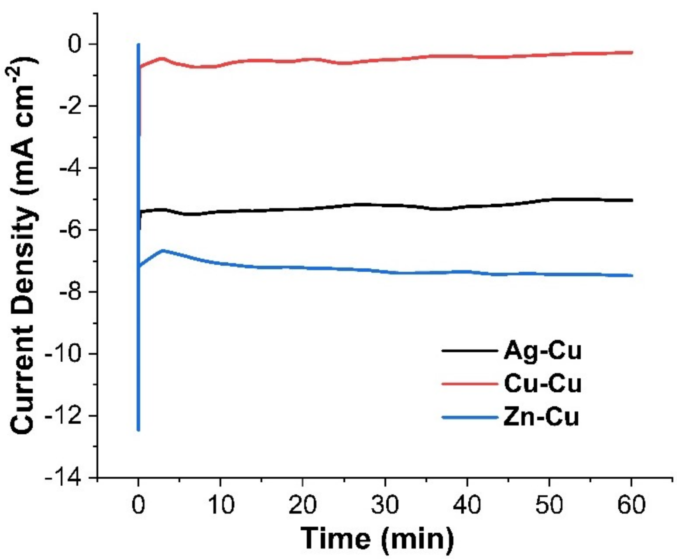

Figure S10: Representative chronoamperometry curves of CO_2 reduction at -1.2 V vs. RHE using Ag-Cu (black), Cu-Cu (red), and Zn-Cu (blue) electrodes.

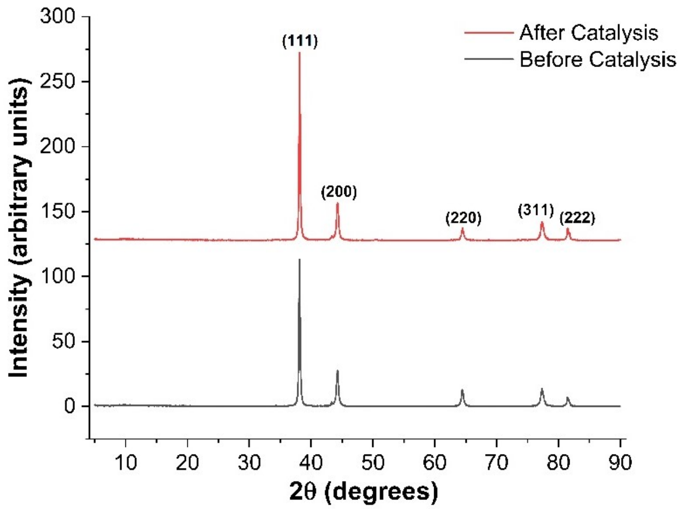

Figure S11: X-ray diffraction spectra before (black) and after (red) CO_2 reduction at -1.2 V vs. RHE using a Ag-Cu electrode modified with 16 μm of Nafion. The Nafion layer was washed away with water before analysis to facilitate the collection.

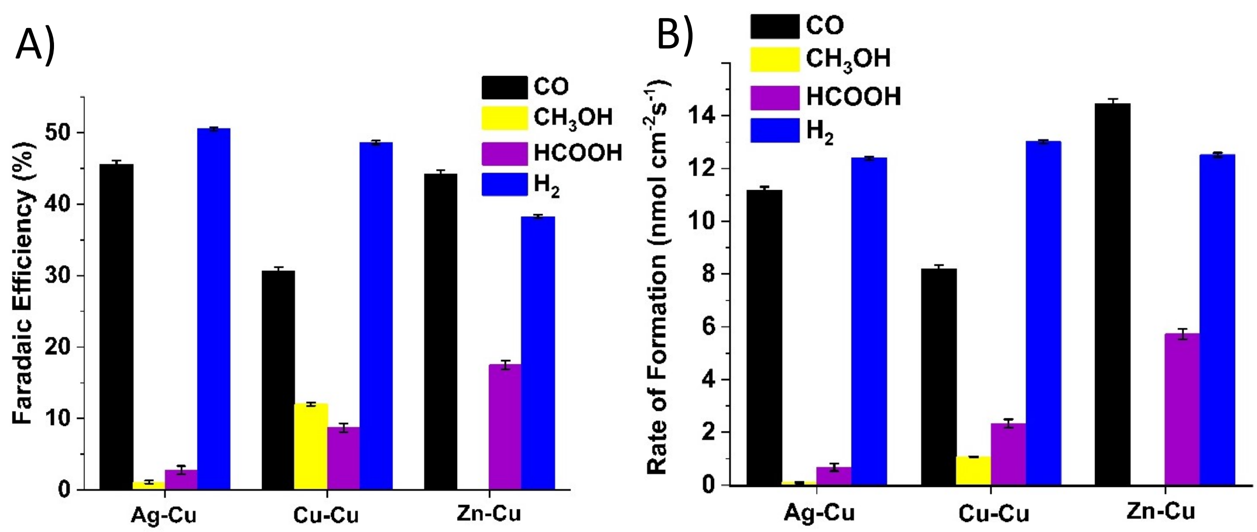

Figure S12: Faradaic efficiencies (A) and rates of formation (B) for CO (black), CH_3OH (yellow), HCOOH (purple), and H_2 (blue) after 1 hr of CO_2 reduction at -1.2 V vs. RHE using Ag-Cu, Cu-Cu, and Zn-Cu.

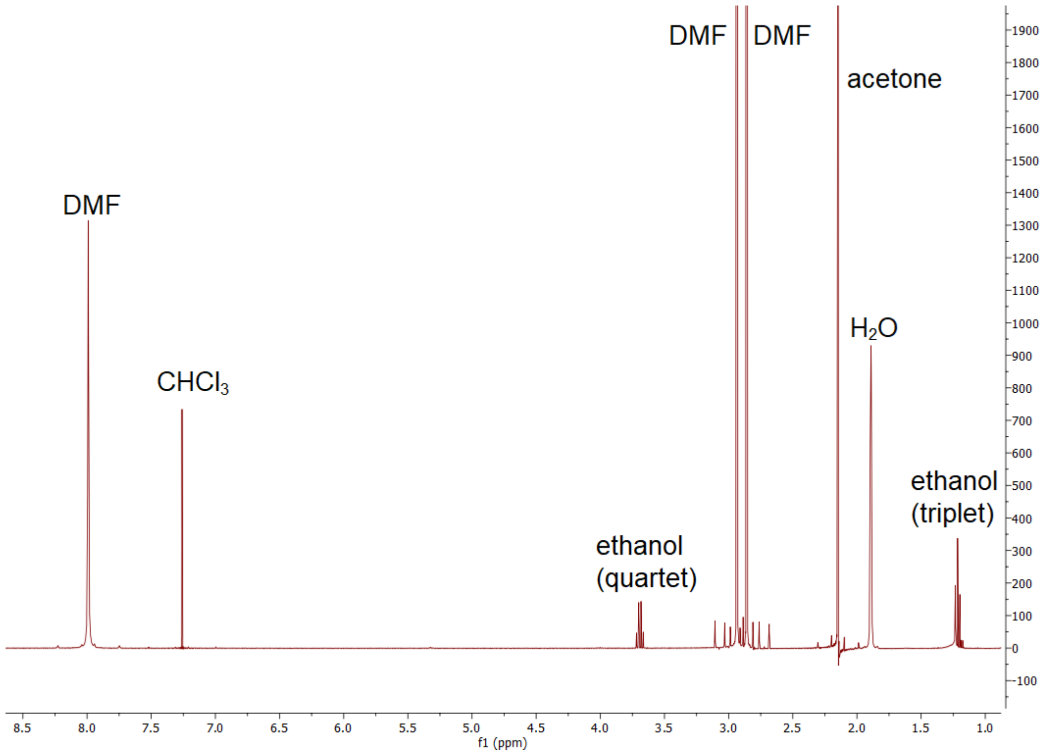

Figure S13: [1]H NMR spectroscopy confirming ethanol production after 1 hr of CO_2 reduction at -1.2 V vs. RHE using the Ag-Cu electrode modified with 16 μm of Nafion. In addition to the produced ethanol, the [1]H NMR spectrum contains the added DMF internal standard, residual $CHCl_3$ from the $CDCl_3$ NMR solvent, residual H_2O, and residual acetone from the cleaning the NMR tube.

Table S1: Comparison of CO_2 electrocatalysts in the literature with high Faradaic efficiencies for C_2H_5OH.

	% Yield	Catalysts	References
1.	72%	Ag/Cu-Nafion	This work
2.	40%	Wrinkle Cu catalyst with high facets	J. Y. Kim, W. Park, C. Choi, G. Kim, K. M. Cho, J. Lim, S. J. Kim, A. Al-Saggaf, I. Gereige, H. Lee, W. B. Jung, Y. Jung and H. T. Jung, *ACS Catalysis*, 2021, **11**, 5658-5665.
3.	93.2%	Boron and N_2-Co-doped nanodiamond	Y. Liu, Y. Zhang, K. Cheng, X. Quan, X. Fan, Y. Su, S. Chen, H. Zhao, Y. Zhang, H. Yu and M. R. Hoffmann, *Angewandte Chemie International Edition*, 2017, **56**, 15607-15611.
4.	63%	CuNP/CNS	D. Karapinar, C. E. Creissen, J. G. Rivera de la Cruz, M. W. Schreiber and M. Fontecave, *ACS Energy Letters*, 2021, **6**, 694-706.
5.	91%	C supported Cu	H. Xu, D. Rebollar, H. He, L. Chong, Y. Liu, C. Liu, C.-J. Sun, T. Li, J. V. Muntean, R. E. Winans, D. J. Liu and T. Xu, *Nature Energy*, 2020, **5**, 623-632.
6.	51%	Cu_2-CuN_3 cluster	X. Su, Z. Jiang, J. Zhou, H. Liu, D. Zhou, H. Shang, X. Ni, Z. Peng, F. Yang, W. Chen, Z. Qi, D. Wang and Y. Wang, *Nature Communications*, 2022, **13**, 1322.
7.	64%	Cu_3Sn	L. Shang, X. Lv, L. Zhong, S. Li and G. Zheng, *Small Methods*, 2022, **6**, 2101334.
8.	52%	N-doped C on Cu	D. Wakerley, S. Lamaison, J. Wicks, A. Clemens, J. Feaster, D. Corral, S. A. Jaffer, A. Sarkar, M. Fontecave, E. B. Duoss, S. Baker, E. H. Sargent, T. F. Jaramillo and C. Hahn, *Nature Energy*, 2022, **7**, 130-143.
9.	50%	Ag/Cu nano	S. C. Abeyweera, M. Simukaitis, Q. Wei and Y. Sun, *SmartMat*, 2022, **3**, 173-182.
10.	32%	Grain boundary rich Cu	Z. Chen, T. Wang, B. Liu, D. Cheng, C. Hu, G. Zhang, W. Zhu, H. Wang, Z. J. Zhao and J. Gong, *Journal of the American Chemical Society*, 2020, **142**, 6878-6883.
11.	47.2%	CuO/TiO_2	J. Yuan, J. J. Zhang, M. P. Yang, W. J. Meng, H. Wang and J.-X. Lu, 2018, **8**, 171.
12.	85.2%	Ag-N-doped graphene/carbon foam	K. Lv, Y. Fan, Y. Zhu, Y. Yuan, J. Wang, Y. Zhu and Q. Zhang, *Journal of Materials Chemistry A*, 2018, **6**, 5025-5031.